

1           **Subsystem identification in structures with a human occupant**  
2           **based on composite frequency response functions**

3  
4           Xiaojun Wei\*<sup>a, c</sup>, Stana Živanović<sup>b, c</sup>, Justin Russell<sup>c</sup>, John E. Mottershead<sup>d</sup>

5           <sup>a</sup> Department of Mechanical and Vehicle Engineering, Hunan University, Changsha 410082,  
6           China

7           <sup>b</sup> College of Engineering, Mathematics and Physical Sciences, University of Exeter, Exeter,  
8           EX4 4QF, UK

9           <sup>c</sup> School of Engineering, University of Warwick, Coventry, CV4 7AL, UK

10          <sup>d</sup> Department of Mechanical, Materials and Aerospace Engineering, University of Liverpool,  
11          Liverpool, L69 3GH, UK

12                   \*Corresponding author, E-mail: [x.wei.3@warwick.ac.uk](mailto:x.wei.3@warwick.ac.uk)

13  
14                   **Abstract**

15   A method is proposed for the subsystem identification of a composite system composing a  
16   **lightweight low-frequency** civil engineering structure and a human occupant. It is shown for  
17   the first time that the dynamics of the structure and the stiffness and damping of the human  
18   occupant can be determined from the frequency response functions of the composite system  
19   and the known mass of the human occupant. The advantage of the proposed approach over  
20   existing methods is not only in the simplicity of problem formulation but also in the substantial  
21   reduction of experimental complexity. Subsystem identification is demonstrated using a  
22   numerical example and two experimental case studies. In the first experimental case study, the  
23   method is applied to a laboratory bridge with a human occupant in a standing posture and  
24   frequency response functions are measured using shaker testing. In the second case study, the  
25   method is applied to a laboratory bridge with a hammer operator crouching on the bridge to  
26   perform impact hammer tests. It is demonstrated that subsystem dynamics can be accurately  
27   identified. The method is especially applicable to the correction of the effect of the hammer  
28   operator in manually operated impact hammer testing. **In addition, the method can be**

29 generalised for the compensation of the effects of the electrodynamic shaker in shaker testing  
30 for civil engineering applications.

31 **Keywords:** Human-structure interaction; subsystem identification; impact hammer testing;  
32 frequency response function.

### 33 1. Introduction

34 Human-structure interaction is a well-recognised phenomenon which involves the interplay of  
35 the dynamics of the two subsystems in human-structure systems, i.e. the human occupant(s)  
36 and the structure supporting the human occupant(s). This mechanism can lead to various  
37 modifications of the dynamic properties of the structure, including the increase [1, 2] or  
38 decrease [1-4] of natural frequencies, increase [1-4] or decrease [2] of damping ratios, and even  
39 the appearance of new modes [1, 2]. The actual change of dynamic properties and the extent of  
40 human-structure interaction are dependent upon the mass, damping and frequency ratios  
41 between the occupant(s) and the structure [2, 5].

42 The effect of human-structure interaction has become of major importance in vibration  
43 serviceability design of lightweight and slender structures in the last two decades [1, 6-9]. In  
44 structural design applications, the dynamics of the human body are commonly represented by  
45 a single degree of freedom (SDOF) mass-spring-damper model [10-18]. The research mainly  
46 concerns identifying human body dynamics [10-18] and predicting the dynamics of human-  
47 structure systems [5, 18-22]. The human body dynamics may be identified directly by curve  
48 fitting measured driving-point apparent masses [11, 12] or derived indirectly from the known  
49 dynamics of the empty structure and the human-structure system [10, 13-18]. When the  
50 dynamics of the human occupant and the empty structure are known, the dynamic prediction  
51 of the joint system is relatively straightforward. Specifically, a spatial or modal model of the  
52 joint system is first constructed by combining the known spatial or modal model of the empty  
53 structure and the human model, based on which the dynamic prediction is performed.

54 Manually operated impact hammer testing is another structural engineering application which  
55 involves human-structure interaction. It has been widely utilised for modal analysis of small  
56 and medium civil engineering structures thanks to its convenience, efficiency and economy [23,  
57 24]. For such testing, a hammer operator is present on the structure during the data collection.

58 Consequently, the identified dynamic properties are essentially those of the human-structure  
59 system rather than those of the empty structure. For some lightweight low-frequency structures,  
60 especially with frequencies close to the frequency of the human body, the influence of the  
61 human occupant can be significant [18, 25]. Unfortunately, existing system identification  
62 methods using data from impact hammer tests routinely neglect the effect of the hammer  
63 operator, which might lead to significant errors in the dynamic identification of the empty  
64 structure. Little attention has been paid to the elimination of the effect of the hammer operator  
65 in impact hammer testing. Recently, Wei and Živanović [18] stressed the importance of the  
66 effect of the hammer operator on the dynamic identification of the empty structure and  
67 presented explicit formulas for deriving the frequency response functions (FRFs) of the empty  
68 structure provided that the human body dynamics and the measured FRFs of the human-  
69 structure system are both known. In addition, other methods for identifying human body  
70 dynamics [13-16] could also be used for the dynamic identification of the empty structure if  
71 the dynamics of the human body and the human-structure system are both known. However,  
72 the aforementioned methods [13-16, 18] require the identification of the dynamics of the  
73 particular hammer operator from laboratory experiments, in which the hammer operator should  
74 keep the same posture as that employed in the on-site impact hammer tests. An alternative  
75 might be to adopt existing human-body models from the literature, but this introduces errors  
76 due to inter- and intra-subject variations [11, 15, 26, 27].

77 This paper proposes a new method for identifying the dynamics of the human body and the  
78 empty structure in a human-structure system, based only on the measured FRFs of the  
79 composite system. A pair of eigenvalues of the empty structure are first identified using three  
80 measured direct FRFs of the structure with a human occupant at three different locations. In  
81 the next step, the human body dynamics are explicitly derived in terms of the identified  
82 eigenvalues of the empty structure and FRFs of the human-structure system. Finally, the FRFs  
83 of the empty structure are explicitly deduced in terms of the FRFs of the human-structure  
84 system and the identified human body dynamics. Therefore, the proposed method is superior  
85 to the existing methods for identifying human body dynamics [10, 13-18] which require  
86 knowledge of both the dynamics of the empty structure and the human-structure system. In  
87 addition, the proposed method is superior to the existing methods for identifying the dynamics  
88 of the empty structure which require knowledge of the human body dynamics, typically  
89 obtained from separate laboratory experiments, and the dynamics of the human-structure  
90 system. **The separate laboratory experiments for identifying human body dynamics require**

91 either a lightweight low-frequency structure by the indirect method [10, 13-18], or a shaker  
92 and a force platform directly [11]. The necessary equipment may not be available to industrial  
93 engineers and even to researchers. The proposed method, requiring only on-site experiments  
94 for obtaining the FRFs of the structure occupied by a human occupant, is more economical  
95 than existing methods and avoids the effects of the inter- and intra-subject variations caused by  
96 adopting standard human-body dynamic models from literature. The proposed method is  
97 especially applicable to the elimination of the effect of the hammer operator in manually  
98 operated impact hammer testing. Additionally, this approach can be generalised to correct the  
99 effects of the electrodynamic shaker in shaker testing. Furthermore, this paper dicusses the  
100 effects of the time delay between the response and force signal measurement on measured FRFs  
101 of the structure under test and proposes appropriate strategies for correcting these effects. This  
102 paper concerns a single human occupant interaction with lightweight low-frequency structures  
103 (i.e. vibration modes with natural frequencies up to about 8 Hz) with well-sperated modes. In  
104 this frequency region, the first vibration mode of the human occupant is likely to interact with  
105 the structure, and therefore the human body is modelled as a SDOF system. The effect of the  
106 uncertainty in human body dynamics on the dynamic identification of the empty structure can  
107 be investigated using the perturbation method presented in the paper [18], therefore it is not  
108 elaborated here.

109 Following this introductory section, Section 2 introduces the theory for the identification of the  
110 dynamics of the human body and the empty structure in a human-structure system. A numerical  
111 illustration of the working of the method is presented in Section 3, whilst its experimental  
112 demonstrations are presented in Section 4. Conclusions are drawn in Section 5.

## 113 **2. Theory**

114 This section presents the theory for the identification of the dynamics of both the human body  
115 and the empty structure from the measured FRFs of a human-structure system.

### 116 **2.1. The relationship between the FRFs of the empty structure and the human-structure** 117 **system**

118 The dynamics of a linear structure having  $n$  DOFs are modified when occupied by a stationary  
119 human. The SDOF dynamics of the human body are represented by mass  $m_h$ , damping  $c_h$  and  
120 stiffness  $k_h$ .  $m_h$  is assumed to represent the physical mass of the human body in line with some

121 previous studies [3, 10, 18, 28-31]. Therefore, the presence of the human occupant introduces  
 122 an additional DOF, denoted as the  $(n + 1)$ -th DOF. Without loss of generality, it is assumed  
 123 that the human occupant is located at the  $p$ -th DOF ( $p \leq n$ ) of the structure. The stiffness and  
 124 damping elements of the human body are connecting the  $p$ -th and  $(n + 1)$ -th DOFs and the  
 125 mass of the human body is considered to be concentrated at the  $(n + 1)$ -th DOF.

126 Wei and Živanović [18] showed that the direct receptance at the  $p$ -th DOF of the empty  
 127 structure  $h_{pp}^s(s)$  and that of the human-structure system  $h_{pp}^{sh,p}(s)$ , where  $s$  is the Laplace  
 128 variable and  $p$  in the superscript indicates the location of the human occupant, may be  
 129 expressed as

$$130 \quad h_{pp}^s(s) = \frac{\left(1 + \frac{1}{m_h s^2}(c_h s + k_h)\right) h_{pp}^{sh,p}(s)}{1 + \frac{1}{m_h s^2}(c_h s + k_h) - (c_h s + k_h) h_{pp}^{sh,p}(s)} \quad (1)$$

131 and the cross receptance between the  $q$ -th DOF ( $q \leq n$ ) and the  $p$ -th DOF of the empty  
 132 structure  $h_{qp}^s(s)$  and that of the human-structure system  $h_{qp}^{sh,p}(s)$  are given by

$$133 \quad h_{qp}^s(s) = h_{qp}^{sh,p}(s) + \frac{h_{qp}^{sh,p}(s)(c_h s + k_h)h_{pp}^{sh,p}(s)}{1 + \frac{1}{m_h s^2}(c_h s + k_h) - (c_h s + k_h)h_{pp}^{sh,p}(s)}. \quad (2)$$

## 134 2.2. Identification of a pair of eigenvalues of the empty structure

135 The denominator of Eq. (1) or (2) generates the characteristic equation

$$136 \quad 1 + \frac{1}{m_h \mu_i^2}(c_h \mu_i + k_h) - (c_h \mu_i + k_h)h_{pp}^{sh,p}(\mu_i) = 0 \quad (3)$$

137 where  $\mu_i$  is the  $i$ -th eigenvalue corresponding the  $i$ -th mode of the empty structure.

138 Similarly, if the human occupant is located at the  $q$ -th DOF of the structure, then

$$139 \quad 1 + \frac{1}{m_h \mu_i^2}(c_h \mu_i + k_h) - (c_h \mu_i + k_h)h_{qq}^{sh,q}(\mu_i) = 0 \quad (4)$$

140 where  $h_{qq}^{sh,q}(s)$  is the direct receptance at the  $q$ -th DOF of the structure with the human  
 141 occupant at the  $q$ -th DOF.

142 Subtracting Eq. (4) from Eq.(3) leads to

$$143 \quad (c_h \mu_i + k_h) \left( h_{qq}^{sh,q}(\mu_i) - h_{pp}^{sh,p}(\mu_i) \right) = 0. \quad (5)$$

144 Since the eigenvalues of an actual underdamped stable structure are complex,

$$145 \quad (c_h \mu_i + k_h) \neq 0. \quad (6)$$

146 Therefore, Eq. (5) is equivalent to

$$147 \quad h_{qq}^{sh,q}(\mu_i) - h_{pp}^{sh,p}(\mu_i) = 0 \quad (7)$$

148 which indicates that the eigenvalues of the empty structure are zeros of the rational function

$$149 \quad \Delta h^{qp}(s) = h_{qq}^{sh,q}(s) - h_{pp}^{sh,p}(s) = 0. \quad (8)$$

150 However,  $\Delta h^{qp}(s)$  generally has additional zeros that are not related to the dynamics of the  
 151 empty structure. The selection of correct eigenvalues for the empty structure requires additional  
 152 checks.

153 Due to relatively small changes of the human-structure system properties compared to the  
 154 properties of the empty structure, the eigenvalues of any particular mode of the empty structure  
 155 will be close to those of the corresponding mode of the human-structure system. Let us assume  
 156 that the  $i$ -th pair of complex conjugate eigenvalues  $\mu_i^s$  and  $\bar{\mu}_i^s$  of the empty structure are the  
 157 targets for identification. The  $i$ -th pair of complex conjugate eigenvalues  $\mu_i^{sh}$  and  $\bar{\mu}_i^{sh}$ ,  
 158 corresponding to the  $i$ -th mode dominated by the structural motion of the human-structure  
 159 system, should be good initial guesses for  $\mu_i^s$  and  $\bar{\mu}_i^s$ , respectively, when solving Eq. (8) by  
 160 using algorithms for solving nonlinear equations, e.g. the trust region algorithm [32]. In the  
 161 frequency range around the  $i$ -th mode dominated by the structural motion of the human-  
 162 structure system, the FRF curves of  $h_{qq}^{sh,q}(s)$  and  $h_{pp}^{sh,p}(s)$  have at most three intersections

163 nearest to their peaks (under the assumption that vibration modes of the empty structure are  
 164 well separated). The zeros of  $\Delta h^{qp}(s)$  related to the dynamics of the empty structure can be  
 165 checked since the correct eigenvalues of the empty structure should also be the zeros of  
 166  $\Delta h^{rp}(s) = h_{rr}^{sh,r}(s) - h_{pp}^{sh,p}(s)$  and  $\Delta h^{rq}(s) = h_{rr}^{sh,r}(s) - h_{qq}^{sh,q}(s)$  where  $h_{rr}^{sh,r}(s)$  is the  
 167 measured direct receptance at the  $r$ -th DOF of the human-structure system with the human  
 168 occupant at the  $r$ -th DOF.

### 169 2.3. Identification of the dynamics of the human body

170 Let us assume that the eigenvalues  $\mu_i^s$  and  $\bar{\mu}_i^s$  of the empty structure have been identified by  
 171 the proposed approach described in Section 2.2. The eigenvalues  $\mu_i^s$  and  $\bar{\mu}_i^s$  should satisfy  
 172 Eq.(3), i.e.

$$173 \begin{bmatrix} c_h \\ k_h \end{bmatrix} = \begin{bmatrix} \mu_i^s & 1 \\ \bar{\mu}_i^s & 1 \end{bmatrix}^{-1} \begin{bmatrix} \frac{(\mu_i^s)^2 m_h}{(\mu_i^s)^2 m_h h_{pp}^{sh,p}(\mu_i^s) - 1} \\ \frac{(\bar{\mu}_i^s)^2 m_h}{(\bar{\mu}_i^s)^2 m_h h_{pp}^{sh,p}(\bar{\mu}_i^s) - 1} \end{bmatrix} \quad (9)$$

174 Eq. (9) infers that the damping  $c_h$  and stiffness  $k_h$  of the human body can be calculated using  
 175 the mass  $m_h$  of the human body and the direct receptance of the human-structure system  
 176  $h_{pp}^{sh,p}(s)$  evaluated at a pair of eigenvalues  $\mu_i^s$  and  $\bar{\mu}_i^s$  of the empty structure. Eq. (9) always  
 177 results in real solutions for  $c_h$  and  $k_h$  due to the use of the complex conjugate pair  $\mu_i^s$  and  $\bar{\mu}_i^s$ .

178 If the measured quantity is accelerance rather than receptance, an alternative form of Eq. (9)  
 179 should be used. It is known that the acceleration  $\mathbf{a}(s)$  and the displacement  $\mathbf{x}(s)$  are related by  
 180  $\mathbf{a}(s) = s^2 \mathbf{x}(s)$ . The receptance matrix  $\mathbf{H}^{sh}(s)$  and the accelerance matrix  $\mathbf{H}_a^{sh}(s)$  satisfy the  
 181 relationship

$$182 \mathbf{H}^{sh}(s) = \frac{\mathbf{H}_a^{sh}(s)}{s^2} \quad (10)$$

183 leading to the estimate of the damping and stiffness of the human from Eq. (11)

184

$$\begin{bmatrix} c_h \\ k_h \end{bmatrix} = \begin{bmatrix} \mu_i^s & 1 \\ \bar{\mu}_i^s & 1 \end{bmatrix}^{-1} \begin{bmatrix} (\mu_i^s)^2 m_h \\ m_h h_{a,pp}^{sh,p} (\mu_i^s)^{-1} \\ (\bar{\mu}_i^s)^2 m_h \\ m_h h_{a,pp}^{sh,p} (\bar{\mu}_i^s)^{-1} \end{bmatrix} \quad (11)$$

185 Note that the same human body dynamics will be identified if any other direct receptance (e.g.  
 186  $h_{qq}^{sh,q}$  or  $h_{rr}^{sh,r}$ ) of the human-structure system is used in Eq. (9) because they are equal to each  
 187 other at the eigenvalues of the empty structure.

#### 188 2.4. Identification of the dynamics of the empty structure

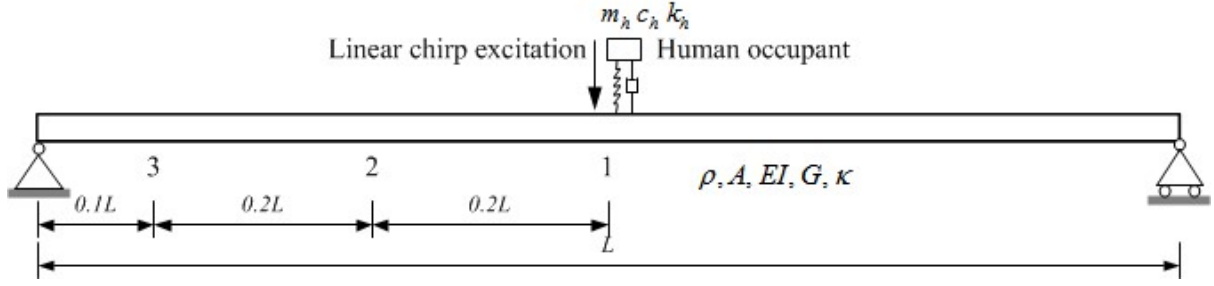
189 The direct and cross receptances of the empty structure can be calculated using Eqs. (1) and  
 190 (2), the human body dynamics and the direct and cross receptances of the human-structure  
 191 system. The frequencies and damping ratios can then be obtained by solving the characteristic  
 192 equation of the receptances of the empty structure. Since the human body dynamics can be  
 193 identified from measured direct receptances of the human-structure system, the dynamics of  
 194 the empty structure can be obtained entirely from measured direct and cross receptances of the  
 195 human-structure system.

### 196 3. Numerical example

197 A numerical example was conducted based on an actual glass fibre reinforced polymer simply  
 198 supported bridge [25]. A schematic of the bridge is shown in Fig. 1. The bridge model has a  
 199 span of  $L = 16.9$  m, density  $\rho = 1.9 \times 10^3$  kg·m<sup>-3</sup>, area of cross section  $A = 4.89 \times 10^{-2}$  m<sup>2</sup>,  
 200 longitudinal modulus of elasticity  $E = 2.47 \times 10^{10}$  N·m<sup>-2</sup>, second moment of area  $I = 3.5 \times$   
 201  $10^{-3}$  m<sup>4</sup>, shear modulus  $G = 3.9 \times 10^9$  N·m<sup>-2</sup> and shear coefficient  $\kappa = 0.08$ . A human  
 202 occupant having mass  $m_h = 62$  kg, natural frequency  $f_h = 5.0$  Hz and damping ratio  $\zeta_h =$   
 203 37.0%, corresponding to the human model for standing posture specified in ISO 5982 [33], is  
 204 assumed to stand on the bridge. The bridge systems with the human occupant located at points  
 205 1, 2 and 3 are designated as the systems SH1, SH2 and SH3, respectively.

206 A two-dimensional finite element (FE) model of the bridge was developed using an improved  
 207 two-node Timoshenko beam finite element [34]. The FE model consisted of 120 elements of  
 208 equal length. Proportional damping  $\mathbf{C} = \alpha \mathbf{M} + \beta \mathbf{K}$  ( $\alpha = \beta = 0.0008$ ) was assumed. Similarly,  
 209 the FE models of the systems SH1, SH2 and SH3 were constructed.





210

211

**Fig. 1 A schematic of a simply supported bridge with a human occupant and a linear chirp excitation at point 1**

212

213

The four FE models were first used for eigenvalue analysis, which generated the modal parameters of the corresponding actual systems. The natural frequencies and damping ratios of the first mode dominated by structural motion are summarised in Table 1. It is shown that while the relative differences of frequencies of the systems SH1, SH2 and SH3 with respect to the fundamental frequency of the empty bridge are -5.4%, -3.3% and -0.4%, respectively, the counterparts of the damping ratios are 392%, 267% and 33%, respectively. It can be seen that the presence of the human occupant can significantly modify the dynamics of the empty bridge and its effect depends upon the human occupant location.

214

215

216

217

218

219

220

221

**Table 1 Modal parameters of the first structural motion dominated mode**

System	Frequency (Hz)	Damping ratio (%)	Relative difference (%)	
			Frequency	Damping ratio
Empty bridge	4.85	1.2	/	/
SH1	4.59	5.9	-5.4	392
SH2	4.69	4.4	-3.3	267
SH3	4.83	1.6	-0.4	33

222

Based on the FE model, the time-domain responses were numerically calculated for the empty bridge driven by a linear chirp excitation force (having magnitude 100 N and sweeping from 1 Hz to 10 Hz) at point 1 for 112 seconds (s) and then left to return to rest over the next 8 s. The actual direct receptance  $h_{11}^s(s)$  of the empty bridge was then calculated using the excitation force and the resultant vertical displacement response at point 1. Similarly, the direct receptances of the systems SH1, SH2 and SH3, i.e.  $h_{11}^{sh,1}(s)$ ,  $h_{22}^{sh,2}(s)$  and  $h_{33}^{sh,3}(s)$ , were calculated. In this example, the direct receptances  $h_{11}^{sh,1}(s)$ ,  $h_{22}^{sh,2}(s)$  and  $h_{33}^{sh,3}(s)$  play the role of known (usually by measurement) FRFs of the systems SH1, SH2 and SH3. These three actual receptances (abbreviated to 'Act' in Fig. 2) are depicted by the thick solid line, thin dash-dotted line and thick dashed line in Fig. 2, respectively. They exhibit different peak frequencies due to the presence of the human occupant at different locations.

223

224

225

226

227

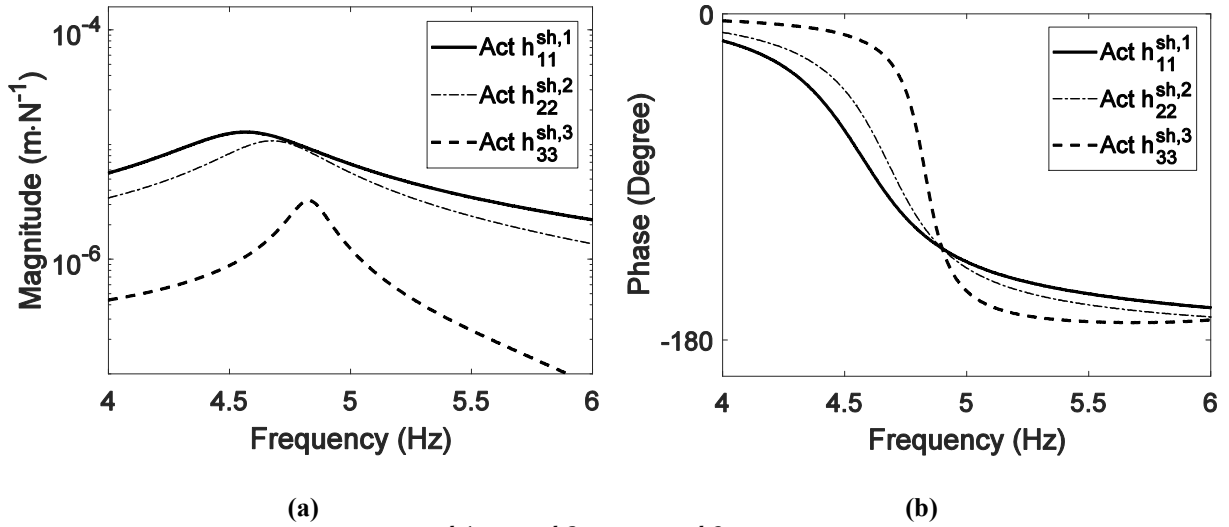
228

229

230

231

232



233 Fig. 2 Direct receptances  $h_{11}^{sh,1}(s)$ ,  $h_{22}^{sh,2}(s)$  and  $h_{33}^{sh,3}(s)$ : (a) Magnitude, (b) Phase

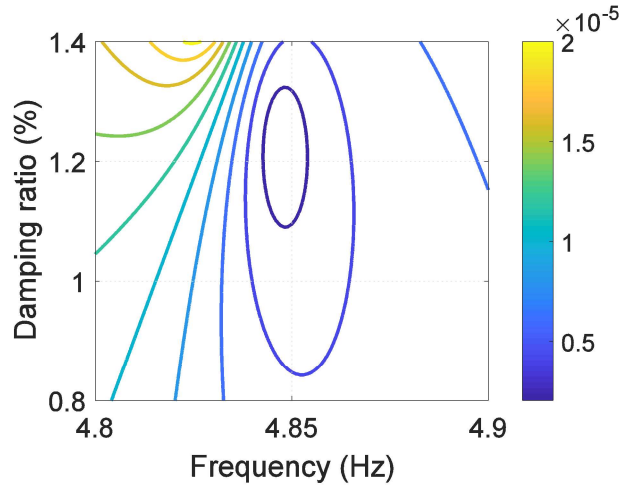
234 The following demonstrates how to identify the subsystem dynamics from the known  
 235 receptances  $h_{11}^{sh,1}(s)$ ,  $h_{22}^{sh,2}(s)$  and  $h_{33}^{sh,3}(s)$ .  $h_{11}^{sh,1}(s)$  was curve fitted in the frequency range  
 236 from 3 Hz to 7 Hz using the rational fraction polynomial method [35], which resulted in an  
 237 analytical expression

$$238 \quad h_{11}^{sh,1} = \frac{a_0 s^6 + a_1 s^5 + a_2 s^4 + a_3 s^3 + a_4 s^2 + a_5 s + a_6}{b_0 s^2 + b_1 s + b_2} \quad (12)$$

239 Where  $a_0 = 2.7933 \times 10^{-12} \text{ s}^4$ ,  $a_1 = -5.2539 \times 10^{-11} \text{ s}^3$ ,  $a_2 = 6.5769 \times 10^{-9} \text{ s}^2$ ,  $a_3 =$   
 240  $-1.9874 \times 10^{-8} \text{ s}$ ,  $a_4 = 6.3407 \times 10^{-7}$ ,  $a_5 = 1.7085 \times 10^{-4} \text{ s}^{-1}$ ,  $a_6 = 0.0277 \text{ s}^{-2}$ ,  $b_0 =$   
 241  $24.1786 \text{ N} \cdot \text{s}^2 \cdot \text{m}^{-1}$ ,  $b_1 = 82.3920 \text{ N} \cdot \text{s} \cdot \text{m}^{-1}$  and  $b_2 = 2.0072 \times 10^4 \text{ N} \cdot \text{m}^{-1}$ . **It should be noted**  
 242 **that the rational expression of  $h_{11}^{sh,1}(s)$  shown in Eq. (12) is improper and cannot be state-**  
 243 **space realisable. Extra numerator polynomial terms in Eq. (12) are used for the compensation**  
 244 **of the residual effects of out-of-band modes such that a good fit is achieved. More information**  
 245 **about the use of this technique in modal parameter identification applications can be found**  
 246 **elsewhere [35].** Its characteristic equation generated the eigenvalue pair  $\mu_{1,2}^{sh,1} = -1.7038 \pm$   
 247  $28.7617i \text{ s}^{-1}$  for the first mode dominated by the structural motion of the system SH1. The  
 248 analytical expressions for  $h_{22}^{sh,2}(s)$  and  $h_{33}^{sh,3}(s)$  were obtained by the same method. Using  
 249  $\mu_{1,2}^{sh,1}$  as the initial guesses, a pair of eigenvalues of the empty bridge was identified as  $\mu_{1,2}^s =$   
 250  $-0.3735 \pm 30.4551i \text{ s}^{-1}$ , i.e. the roots  $s = \mu_{1,2}^s$  of the function

$$251 \quad \Delta h^{13}(s) = h_{11}^{sh,1}(s) - h_{33}^{sh,3}(s) = 0 \quad (13)$$

252  $\mu_{1,2}^s$  were also found to be the zeros of  $\Delta h^{23}(s)$  and  $\Delta h^{12}(s)$ , which confirms  $\mu_{1,2}^s$  were the  
 253 eigenvalues of the empty structure. The corresponding natural frequency and damping ratio  
 254 were then calculated to be 4.85 Hz and 1.2%, which agree with the actual modal parameters of  
 255 the empty bridge given in Table 1. While the magnitude curves of  $h_{11}^{sh,1}(s)$ ,  $h_{22}^{sh,2}(s)$   
 256 and  $h_{33}^{sh,3}(s)$ , shown in Fig. 2(a), do not exhibit their intersections at  $\mu_{1,2}^s$  because the  
 257 intersections are located away from the imaginary axis, their phase curves, shown in Fig. 2(b),  
 258 indicate the intersections.



259

**Fig. 3 The magnitude of  $\Delta h^{13}(s)$  against frequency and damping ratio.**

260

261 In addition, the initial guesses for the solutions to Eq. (13) can be predicted graphically. Fig.  
 262 3 shows the contour map of the magnitude of  $\Delta h^{13}(s)$  against frequency and damping ratio,  
 263 which indicates that values around 4.85 Hz and 1.2% are good initial guesses for the frequency  
 264 and damping ratio of the empty structure, respectively, around which  $\Delta h^{13}(s)$  is at its  
 265 minimum. Note that such a contour map is suggested to be plotted around the eigenvalues of  
 266 the human-structure system since the eigenvalues of any particular mode of the empty structure  
 267 will be close to those of the corresponding mode of the human-structure system.

268

269

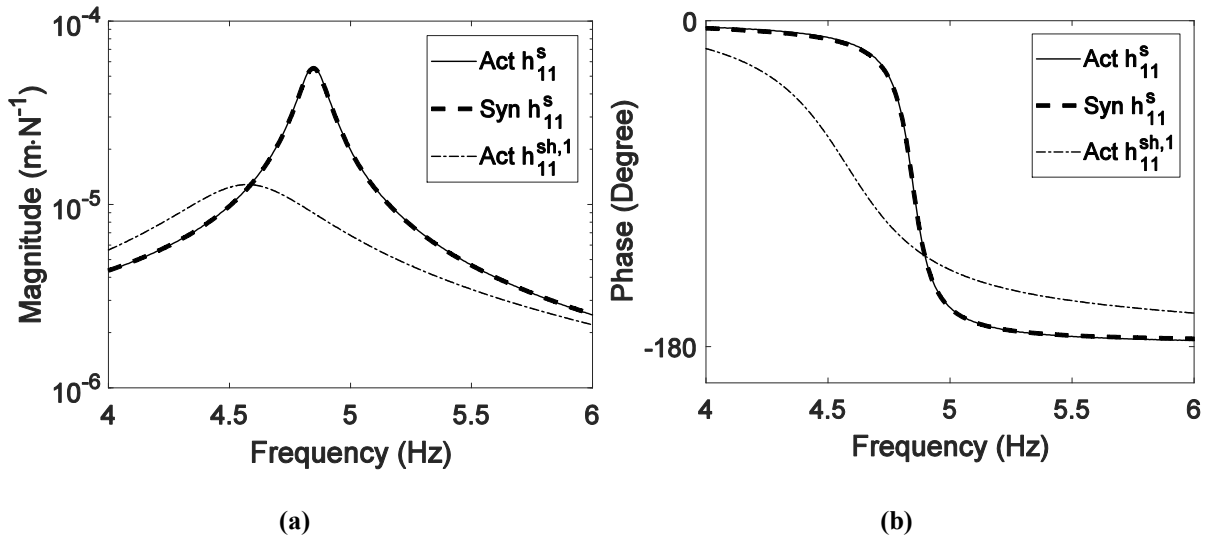
270

Based on the human body mass,  $m_h = 62$  kg, the analytical expression  $h_{11}^{sh,1}(s)$  described by  
 Eq. (12) and the identified eigenvalues  $\mu_{1,2}^s$  of the empty bridge, the damping and stiffness of  
 the human body were calculated as

271

$$\begin{bmatrix} c_h \\ k_h \end{bmatrix} = \begin{bmatrix} \mu_1^s & 1 \\ \mu_2^s & 1 \end{bmatrix}^{-1} \begin{bmatrix} \frac{(\mu_1^s)^2 m_h}{(\mu_1^s)^2 m_h h_{11}^{sh,1}(\mu_1^s) - 1} \\ \frac{(\mu_2^s)^2 m_h}{(\mu_2^s)^2 m_h h_{11}^{sh,1}(\mu_2^s) - 1} \end{bmatrix} = \begin{bmatrix} 1.47 \times 10^3 \text{ N} \cdot \text{s} \cdot \text{m}^{-1} \\ 6.14 \times 10^4 \text{ N} \cdot \text{m}^{-1} \end{bmatrix}.$$

272 The corresponding frequency and damping ratio of the human body were then calculated as  
 273  $f_h = 5.0$  Hz and  $\zeta_h = 37.0\%$ , which are exactly the properties of the actual human occupant  
 274 stated at the outset.



(a) (b)  
 Fig. 4 Direct receptances of SH1 and the empty structure: (a) Magnitude, (b) Phase

275 The direct receptance at point 1 of the empty bridge was then synthesised using Eq.(1), denoted  
 276 as  $Syn h_{11}^s(s)$  and shown by the thick dashed curve in Fig. 4. The synthesised receptance is in  
 277 good agreement with its actual counterpart (abbreviated to ‘Act’ and depicted by the thin solid  
 278 curve in Fig. 4). By solving the characteristic equation for  $Syn h_{11}^s(s)$  the fundamental  
 279 frequency and damping ratio of the empty bridge were found to be 4.85Hz and 1.2%, which  
 280 agree with the actual counterparts of the empty bridge. Similarly, the receptances  $h_{22}^s(s)$  and  
 281  $h_{33}^s(s)$  of the empty structure were also obtained. The three direct receptances of the empty  
 282 structure exhibited the same peak frequency after the elimination of the effect of the human  
 283 occupant.  
 284

#### 285 4. Experimental case studies

286 This section presents two experiments for verifying the theory of subsystem identification. The  
 287 first experiment aims to identify the dynamics of the subsystems of a steel-concrete composite  
 288 bridge with a human occupant in a standing posture. In this experiment, FRFs were measured  
 289 by using shaker testing. The second experiment demonstrates how to eliminate the effect of the  
 290 hammer operator in manually operated impact hammer testing performed on the same bridge.  
 291 The experiments were approved by the Biomedical and Scientific Research Ethics Committee  
 292 at the University of Warwick.

293 **4.1. Subsystem identification using measured FRFs from shaker testing**

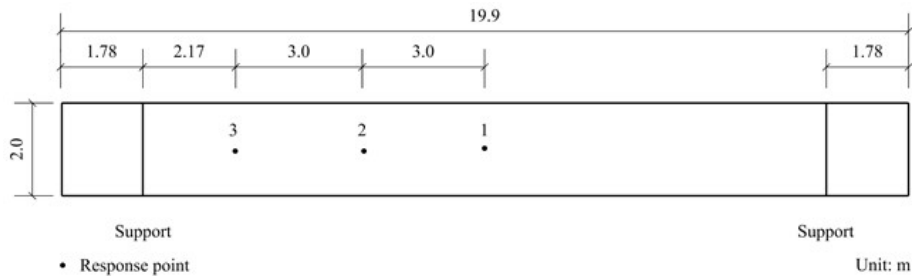
294 A steel-concrete composite bridge situated in the Structures Laboratory at the University of  
295 Warwick (Fig. 5) with a human occupant in a standing posture was considered for subsystem  
296 identification. The bridge is 19.9 m long and 2 m wide and sits on two meccano frames with  
297 1.78 m overhang at each end. The bridge and the human occupant weigh 16,500 kg and 100  
298 kg, respectively.

299 **4.1.1. Shaker testing**

300 The accelerances of the empty bridge and the human-bridge system were measured using  
301 shaker testing. The test points (TPs) are shown in Fig. 6. An electrodynamic shaker of mass  
302 105.5 kg (Model APS 400), as shown in Fig. 5, was placed sequentially at TPs 1, 2 and 3 on  
303 the deck to excite the bridge. The generated force was indirectly measured using an  
304 accelerometer (Honeywell QA750, nominal sensitivity 1300 mV/g) attached to the moving  
305 armature. Another three accelerometers of the same type were placed at TPs 1, 2 and 3 to  
306 measure the vibration responses of the unoccupied bridge and the human-bridge systems in the  
307 vertical direction. The data acquisition system consisted of a laptop, a 16-channel data logger  
308 (SignalCalc Mobilyser by Data Physics), a signal conditioner and a power amplifier (Model  
309 APS 145). A chirp excitation force in the frequency range 1 - 9 Hz was applied to the structure  
310 for 64 seconds. A data acquisition window was set to 128 seconds. The sampling frequency  
311 was 512 Hz. Four averages were used to minimise the effects of noise. No window was used  
312 since the vibration responses returned to the ambient vibration level at the end of the acquisition  
313 window. The typical standing posture of the human is shown in Fig. 7.



314 **Fig. 5 The bridge with the shaker at TP1**



316  
317

**Fig. 6 Bridge deck geometry and test points**



318  
319

**Fig. 7 The bridge with the shaker and the human occupant at TP1**

320 The bridge systems with the exciter (shaker) located at TPs 1, 2 and 3 are designated as the  
 321 systems SE1, SE2 and SE3, respectively. The bridge systems with the human occupant and the  
 322 shaker at TPs 1, 2 and 3 are designated as the systems SHE1, SHE2 and SHE3, respectively.  
 323 The bridge systems with the human occupant at TPs 1, 2 and 3 are designated as the systems  
 324 SH1, SH2 and SH3, respectively.

325 The systems SE1, SE2, SE3, SHE1, SHE2 and SHE3 were excited at three different force levels.  
 326 The maximum accelerations at TP1 of SE1, TP2 of SE2 and TP3 of SE3 ranged from  $0.30 \text{ m}\cdot\text{s}^{-2}$   
 327  $^2$  to  $0.70 \text{ m}\cdot\text{s}^{-2}$ , from  $0.22 \text{ m}\cdot\text{s}^{-2}$  to  $0.50 \text{ m}\cdot\text{s}^{-2}$  and from  $0.14 \text{ m}\cdot\text{s}^{-2}$  to  $0.32 \text{ m}\cdot\text{s}^{-2}$ , respectively.  
 328 The maximum accelerations at TP1 of SHE1, TP2 of SHE2 and TP3 of SHE3 ranged from  
 329  $0.27 \text{ m}\cdot\text{s}^{-2}$  to  $0.68 \text{ m}\cdot\text{s}^{-2}$ , from  $0.21 \text{ m}\cdot\text{s}^{-2}$  to  $0.49 \text{ m}\cdot\text{s}^{-2}$  and from  $0.13 \text{ m}\cdot\text{s}^{-2}$  to  $0.28 \text{ m}\cdot\text{s}^{-2}$ ,  
 330 respectively. The frequencies and damping ratios of SE1 showed negligible variation with the  
 331 response level. The same conclusion was drawn for SE2, SE3, SHE1, SHE2 and SHE3. These  
 332 findings suggest that the systems SE1, SE2, SE3, SHE1, SHE2 and SHE3 exhibited linear  
 333 behaviour in the observed amplitude range. Therefore, it is reasonable to assume that the human  
 334 body exhibited linear behaviour during the testing as well. The force level when excited at TP2  
 335 of SHE2 chosen for presentation in this paper is shown in Fig. 8 whilst the corresponding  
 336 vibration response at TP2 is shown in Fig. 9.

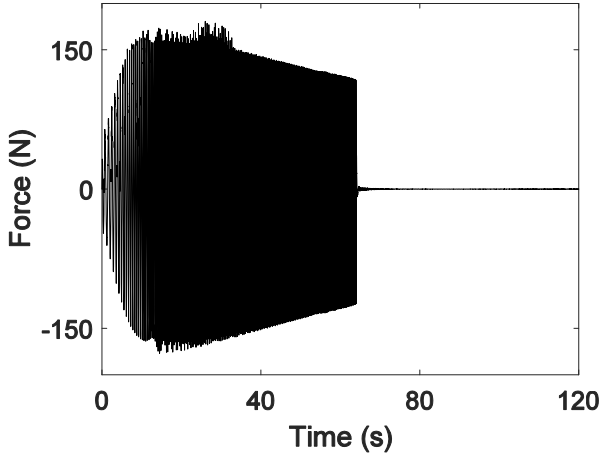


Fig. 8 Excitation force at TP2 of SHE2

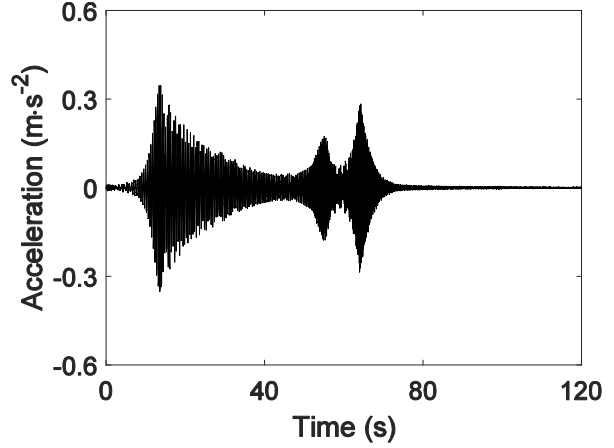


Fig. 9 Acceleration at TP2 of SHE2

337 While the direct accelerances at TP1 of SE1, TP2 of SE2 and TP3 of SE3, denoted as  $h_{a,11}^{se,1}$ ,  
 338  $h_{a,22}^{se,2}$  and  $h_{a,33}^{se,3}$ , respectively, are shown in Fig. 10, the cross accelerances of SE1, excited at  
 339 TP1 and measured at TP3, and of SE3, excited at TP3 and measured at TP1, denoted as  $h_{a,31}^{se,1}$   
 340 and  $h_{a,13}^{se,3}$ , respectively, are shown in Fig. 11. The direct accelerances at TP1 of SHE1, TP2 of  
 341 SHE2 and TP3 of SHE3, denoted as  $h_{a,11}^{she,1}$ ,  $h_{a,22}^{she,2}$  and  $h_{a,33}^{she,3}$  respectively, are shown in Fig.  
 342 12. Fig. 10 and Fig. 11 show that the presence of the shaker on the deck slightly modifies the  
 343 dynamics of the bridge under test, i.e. it shifts the natural frequency and affects the reciprocity  
 344 check. Therefore, the effect of the shaker should be first eliminated from the measured  
 345 accelerances shown in Fig. 12 before they are used to identify the dynamics of the human body  
 346 and the empty bridge.

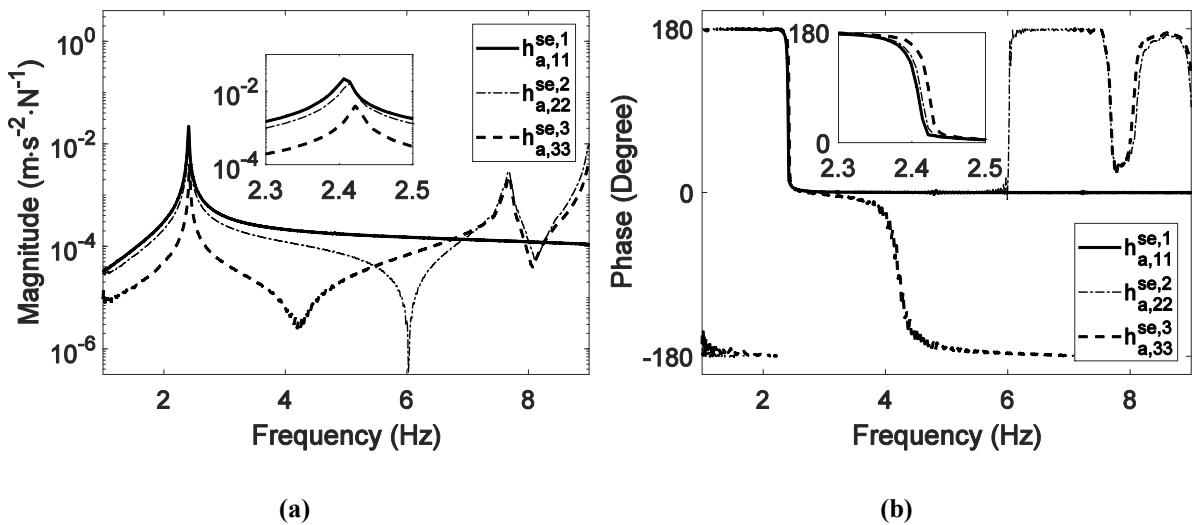
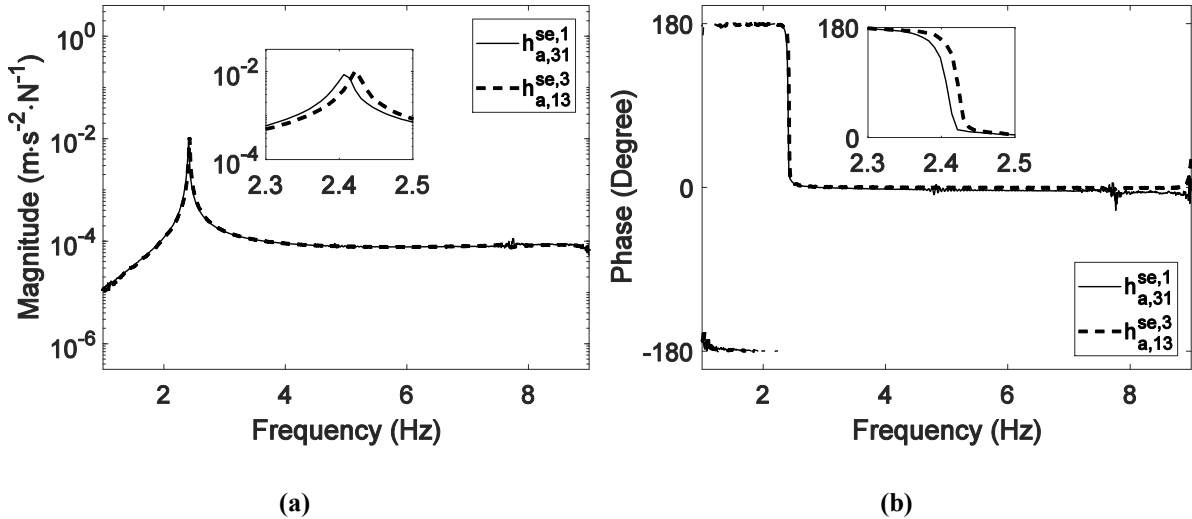
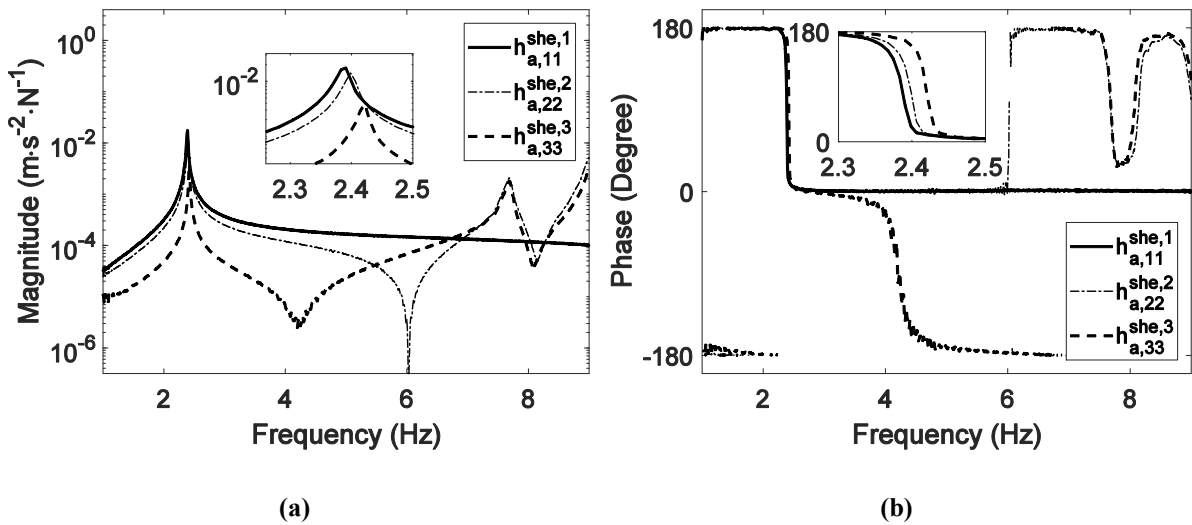


Fig. 10 Measured direct accelerances of the bridge with shaker: (a) Magnitude; (b) Phase



348 Fig. 11 Measured cross accelerances of the bridge with shaker: (a) Magnitude; (b) Phase

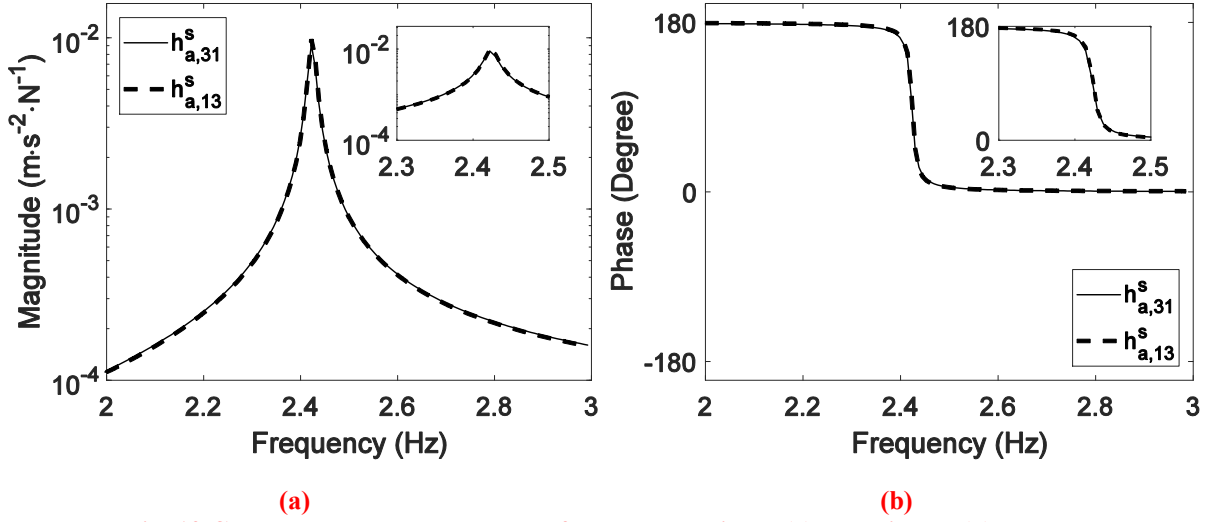


349 Fig. 12 Measured direct accelerances of the bridge with human occupant and shaker: (a) Magnitude; (b)  
350 Phase

#### 351 4.1.2. The elimination of the effect of the electrodynamic shaker

352 The electrodynamic shaker concentrates the majority of its mass on its base (79 kg), while the  
353 moving mass is only 26.5 kg. In this research, the shaker is modelled as a mass block of 105.5  
354 kg. By using Eqs. (21) and (22) from Appendix A, the effect of the shaker on the measured  
355 accelerances of the empty bridge can be eliminated. Fig. 13 shows the corrected cross  
356 accelerances  $h_{a,31}^S$  (thin solid curve) and  $h_{a,13}^S$  (thick dashed curve) of the empty bridge, which  
357 indicate that the principle of reciprocity is now satisfied. In addition, the natural frequency and  
358 damping ratio identified from the corrected accelerances of the empty bridge agree well with  
359 the measured counterparts from impact hammer testing in which the hammer operator stood  
360 next to the bridge.



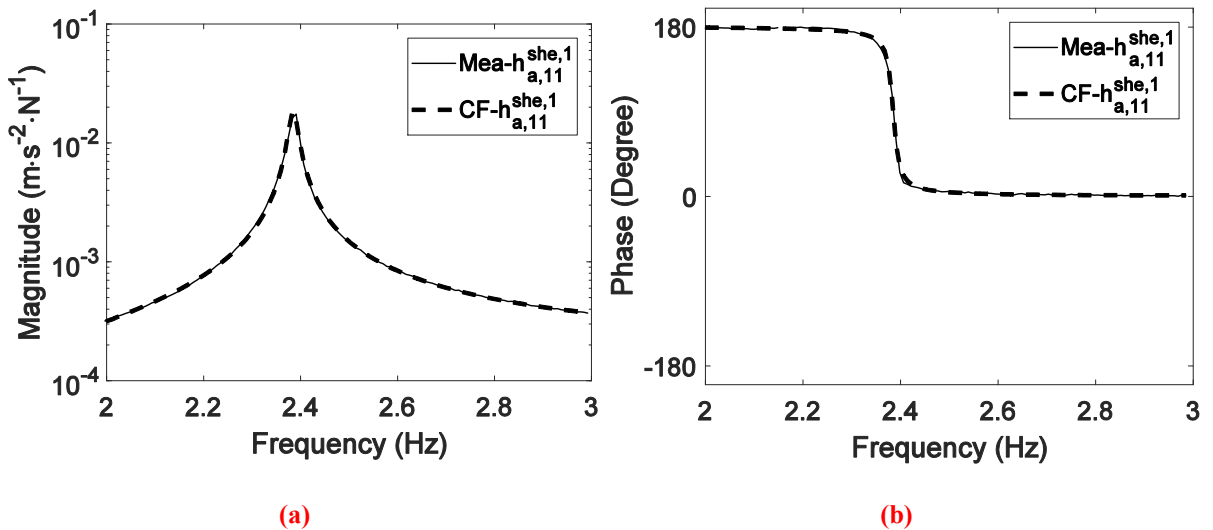


361 **Fig. 13 Corrected cross accelerances of the empty bridge: (a) Magnitude; (b) Phase**

362 Similarly, the effect of the shaker embedded in the measured accelerances  $h_{a,11}^{she,1}$ ,  $h_{a,22}^{she,2}$ ,  $h_{a,33}^{she,3}$ ,  
 363  $h_{a,31}^{she,1}$  and  $h_{a,13}^{she,3}$  can be eliminated. For instance, the measured acceleration of SHE1  $h_{a,11}^{she,1}$   
 364 was first curve fitted using the rational fraction polynomial method [35]. Good agreement  
 365 between the curve-fitted accelerance (thick dashed curve) and its measured counterpart (thin  
 366 solid curve) is demonstrated in Fig. 14. The analytical expression of the curve-fitted  
 367 accelerance is

$$368 \quad h_{a,11}^{she,1}(s) = \frac{a_0 s^2 + a_1 s + a_2}{b_0 s^2 + b_1 s + b_2} \quad (14)$$

369 where  $a_0 = 2.4738 \times 10^{-4}$ ,  $a_1 = -1.2842 \times 10^{-5} \text{ s}^{-1}$ ,  $a_2 = -1.6082 \times 10^{-5} \text{ s}^{-2}$ ,  $b_0 =$   
 370  $1.8417 \text{ N}\cdot\text{s}^2\cdot\text{m}^{-1}$ ,  $b_1 = 0.1967 \text{ N}\cdot\text{s}\cdot\text{m}^{-1}$  and  $b_2 = 413.4934 \text{ N}\cdot\text{m}^{-1}$ .



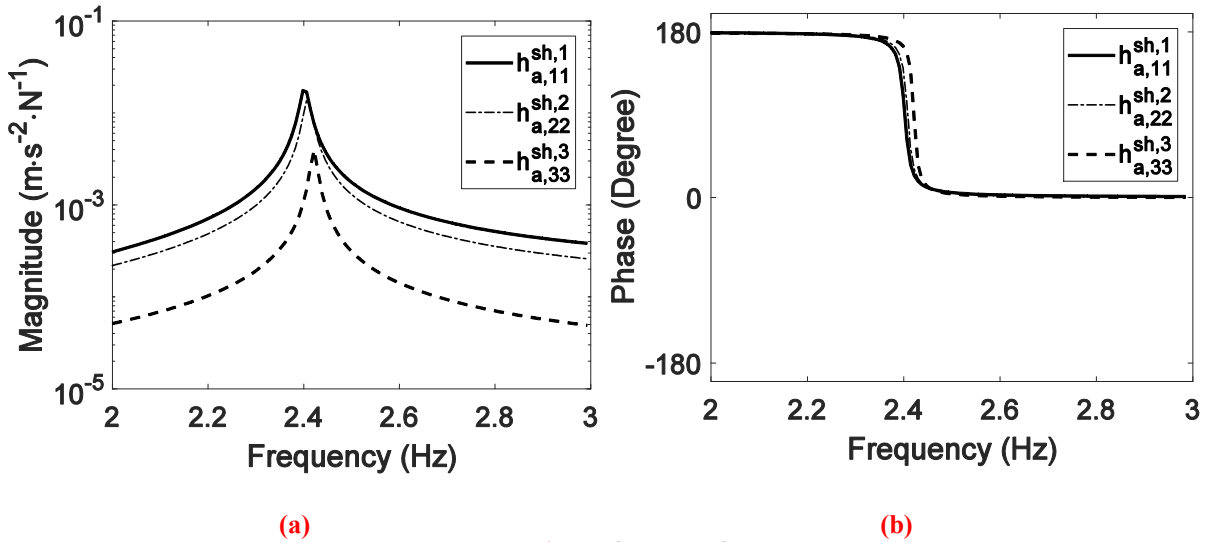
371 **Fig. 14 Comparison between measured and curve-fitted accelerances  $h_{a,11}^{she,1}$ : (a) Magnitude; (b) Phase**

372 According to Eq. (21) from Appendix A, the direct accelerance at TP1 of SH1  $h_{a,11}^{sh,1}$  may be  
 373 synthesised as

$$374 \quad h_{a,11}^{sh,1}(s) = \frac{a_0 s^2 + a_1 s + a_2}{b_0 s^2 + b_1 s + b_2} \quad (15)$$

375 where  $a_0 = 2.4765 \times 10^{-4}$ ,  $a_1 = -1.2855 \times 10^{-5} \text{ s}^{-1}$ ,  $a_2 = -1.6099 \times 10^{-5} \text{ s}^{-2}$ ,  $b_0 =$   
 376  $1.8176 \text{ N}\cdot\text{s}^2\cdot\text{m}^{-1}$ ,  $b_1 = 0.1983 \text{ N}\cdot\text{s}\cdot\text{m}^{-1}$  and  $b_2 = 413.9403 \text{ N}\cdot\text{m}^{-1}$ .

377 Similarly, the accelerances  $h_{a,22}^{sh,2}$ ,  $h_{a,33}^{sh,3}$ ,  $h_{a,31}^{sh,1}$  and  $h_{a,13}^{sh,3}$  were synthesised. The corrected  
 378 accelerances  $h_{a,11}^{sh,1}$ ,  $h_{a,22}^{sh,2}$  and  $h_{a,33}^{sh,3}$  are shown in Fig. 15, in which the peak shift was induced by  
 379 the presence of the human occupant at different locations only.

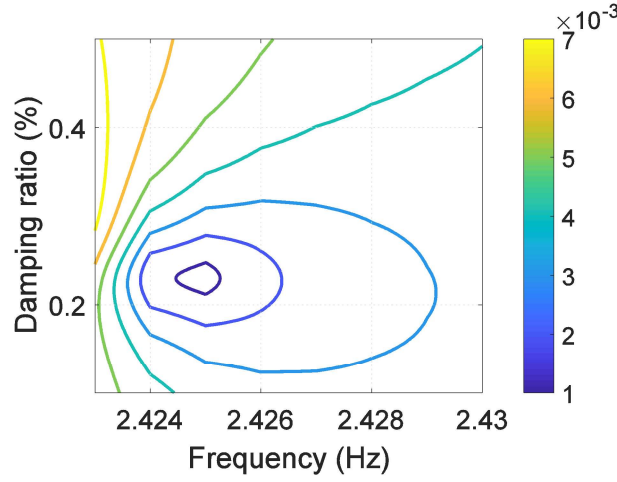


380 **Fig. 15 Comparison of corrected  $h_{a,11}^{sh,1}$ ,  $h_{a,22}^{sh,2}$  and  $h_{a,33}^{sh,3}$ : (a) Magnitude; (b) Phase**

### 381 4.1.3. The identification of the dynamics of the human body and the empty structure

382 A pair of eigenvalues of the human-bridge system SH1 may be obtained as  $\mu_{1,2}^{sh,1} = -0.0545 \pm$   
 383  $15.0910i \text{ s}^{-1}$  by solving the characteristic equation of  $h_{a,11}^{sh,1}$ . Using  $\mu_{1,2}^{sh,1}$  or the points around  
 384 the minimum point in Fig. 16 as the initial guesses for the zeros of  $\Delta h^{13}(s) = h_{a,11}^{sh,1}(s) -$   
 385  $h_{a,33}^{sh,3}(s)$ , a pair of eigenvalues may be obtained as  $\mu_{1,2}^s = -0.0351 \pm 15.2338i \text{ s}^{-1}$ , which were  
 386 also found to be zeros of  $\Delta h^{12}(s)$  and  $\Delta h^{23}(s)$ . This confirms that  $\mu_{1,2}^s$  were the eigenvalues  
 387 of the empty bridge. The corresponding frequency and damping ratio were calculated to be

388 2.42 Hz and 0.23%, which agree well with the measured counterparts from impact hammer  
 389 testing in which the hammer operator stood next to the bridge.



390

391 **Fig. 16 The magnitude of  $\Delta h^{13}(s)$  against frequency and damping ratio**

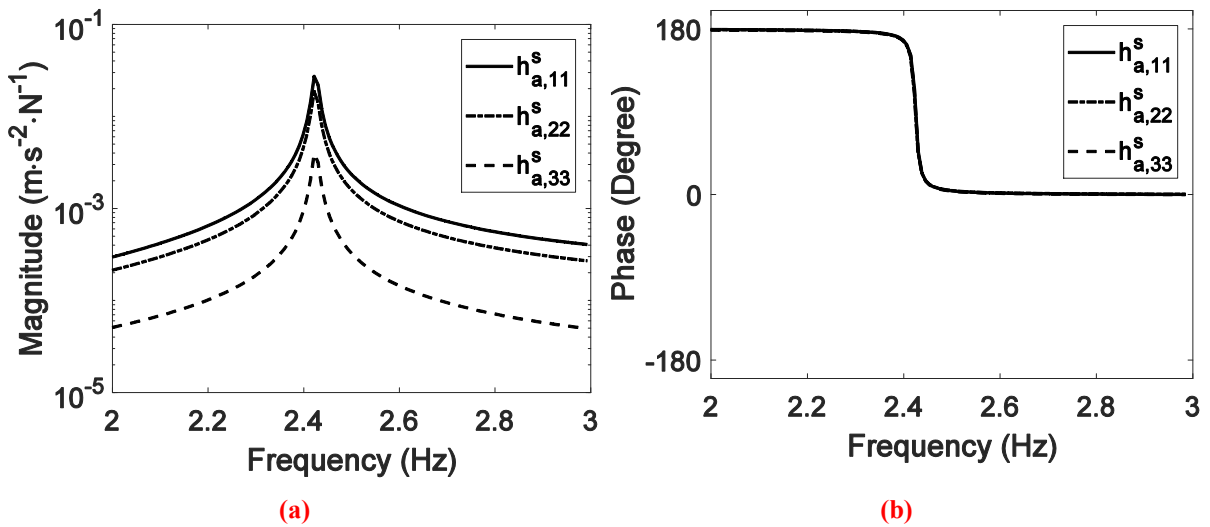
392 Based on the analytical expression of  $h_{a,11}^{sh,1}$  given by Eq.(15), the identified eigenvalues of the  
 393 empty bridge and the human mass ( $m_h = 100$  kg), the damping and stiffness of the human  
 394 body were calculated as

$$395 \quad \begin{bmatrix} c_h \\ k_h \end{bmatrix} = \begin{bmatrix} \mu_1^s & 1 \\ \mu_2^s & 1 \end{bmatrix}^{-1} \begin{bmatrix} \frac{(\mu_1^s)^2 m_h}{m_h h_{a,11}^{sh,1} (\mu_1^s)^{-1}} \\ \frac{(\mu_2^s)^2 m_h}{m_h h_{a,11}^{sh,1} (\mu_2^s)^{-1}} \end{bmatrix} = \begin{bmatrix} 1.75 \times 10^3 N \cdot s \cdot m^{-1} \\ 7.21 \times 10^4 N \cdot m^{-1} \end{bmatrix} \quad (16)$$

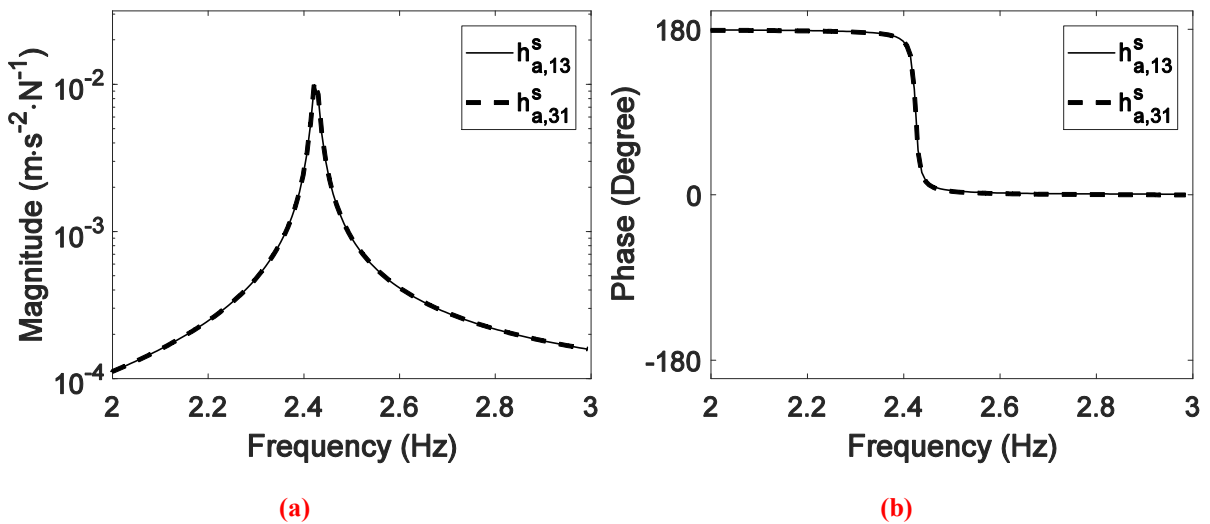
396 from which the corresponding frequency and damping ratio were calculated to be  $f_h = 4.27$   
 397 Hz and  $\zeta_h = 33\%$ , respectively. These results are in the ranges of natural frequency and  
 398 damping ratio for a human body in a standing posture available in the literature [20].

399 Based on the corrected accelerances  $h_{a,11}^{sh,1}$ ,  $h_{a,22}^{sh,2}$ ,  $h_{a,33}^{sh,3}$ ,  $h_{a,31}^{sh,1}$  and  $h_{a,13}^{sh,3}$ , the identified human  
 400 body dynamics and Eqs. (1) and (2), the direct accelerances  $h_{a,11}^s$ ,  $h_{a,22}^s$  and  $h_{a,33}^s$  and the cross  
 401 accelerances  $h_{a,13}^s$  and  $h_{a,31}^s$  of the empty bridge can be synthesised, which are shown in Fig.  
 402 17 and Fig. 18. As can be seen from Fig. 17, the three direct accelerances of the empty bridge  
 403 exhibit the same frequency. Fig. 18 implies that the principle of structural reciprocity is  
 404 satisfied. In addition, the accelerances obtained by eliminating the effect of the shaker from the  
 405 measured accelerances of the bridge with the shaker agree well with those obtained by  
 406 eliminating the effects of the shaker and human occupant from the measured accelerances of

407 the bridge with the human occupant and shaker. These suggest that the effects of the human  
 408 occupant and shaker have been eliminated correctly.



409 **Fig. 17 Synthesised direct accelerances  $h_{a,11}^s$ ,  $h_{a,22}^s$  and  $h_{a,33}^s$  of the empty bridge: (a) Magnitude; (b)**  
 410 **Phase**



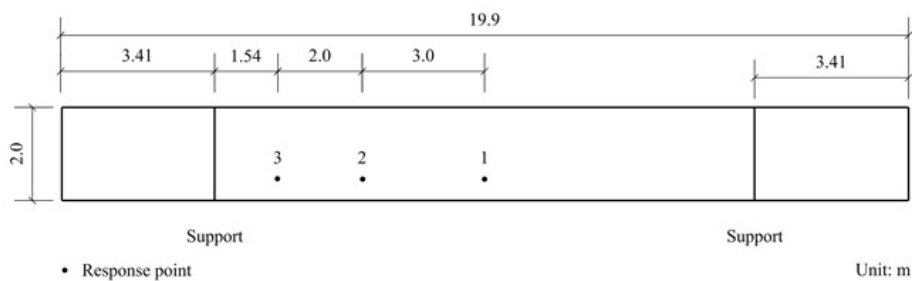
411 **Fig. 18 Synthesised cross accelerances  $h_{a,13}^s$  and  $h_{a,31}^s$  of the empty bridge: (a) Magnitude; (b)**  
 412 **Phase**

412 **4.2. The elimination of the effect of hammer operator in manually operated impact**  
 413 **hammer testing**

414 The same steel-concrete composite bridge used in Section 4.1 was considered again, but with  
 415 3.41 m overhang at each end, i.e. a span length of 13.08 m. The accelerances of the empty  
 416 bridge and the hammer operator-bridge system were measured using manually operated impact  
 417 hammer testing. The TPs are shown in Fig. 19.

418 **4.2.1. Manually operated impact hammer testing**

419 To obtain the accelerances of the empty bridge, the hammer operator stood next to the bridge  
420 to impact sequentially at TPs 1, 2 and 3 on the deck using an instrumented sledge hammer  
421 (Dytran Model 5803A, sensitivity 0.231 mV/N). Three accelerometers (Honeywell QA750,  
422 nominal sensitivity 1300 mV/g) were placed at TPs 1, 2 and 3 to measure the vibration  
423 responses of the empty bridge in the vertical direction. The data acquisition system consisted  
424 of a laptop, a 16-channel data logger (SignalCalc Mobilyser by Data Physics) and a signal  
425 conditioner. The sampling frequency was chosen to be 1024 Hz and the data acquisition  
426 window was set to 64 seconds. Four averages were used to minimise the effects of noise. No  
427 window was used since the vibration responses returned to the ambient vibration level at the  
428 end of the acquisition window. The accelerance measurement of the hammer operator-bridge  
429 system was performed in the same way. The only difference was that the hammer operator  
430 crouched on the deck (sequentially close to at TPs 1, 2 and 3) to perform the impact hammer  
431 testing. The typical crouching posture of the hammer operator is shown in Fig. 20. The hammer  
432 operator and the hammer weigh 62 kg and 5.5 kg, respectively. The bridge systems with the  
433 hammer operator crouching at TPs 1, 2 and 3 are designated as the systems SH1, SH2 and SH3,  
434 respectively.



435

436

**Fig. 19 Bridge deck geometry and test points**

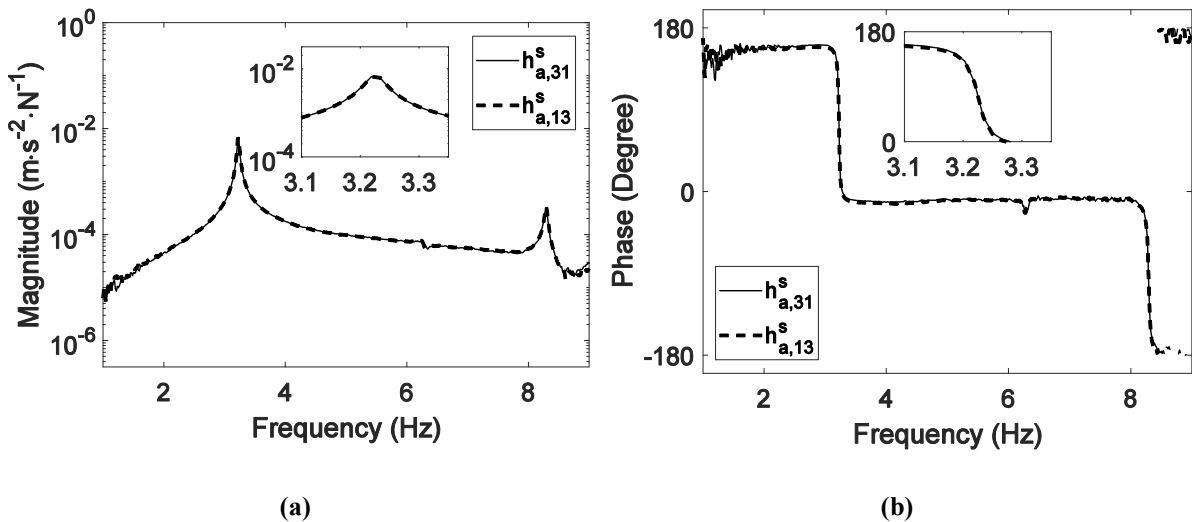


437

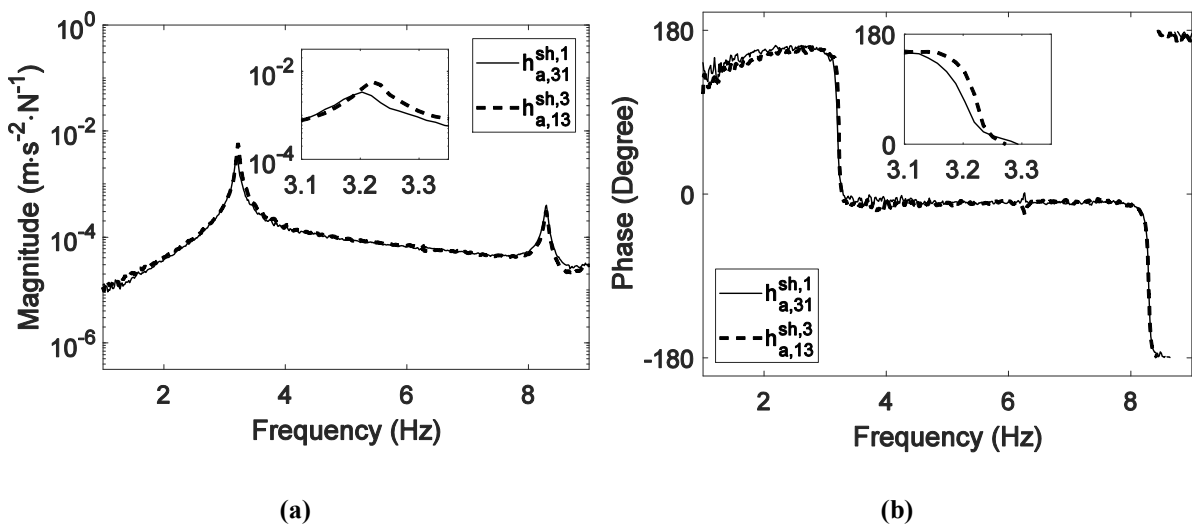
438

**Fig. 20 The bridge with the hammer operator crouching at TP2**

439 The measured cross accelerances  $h_{a,13}^s$  and  $h_{a,31}^s$  of the empty bridge are compared in Fig. 21.  
 440 It can be seen that the reciprocity holds for the empty bridge, which indicates that the dynamic  
 441 behaviour of the bridge was linear in the response range of the tests. The bridge with the  
 442 hammer operator crouching at TPs 1, 2 or 3 was also found to behave linearly by using shaker  
 443 testing. The response range of the shaker tests covers the range of the responses, bandpass  
 444 filtered with cutoff frequencies 2 Hz and 6 Hz, of the impact hammer tests. Therefore, it is  
 445 reasonable to assume that the dynamics of the hammer operator is linear during the testing. Fig.  
 446 22 shows that the cross accelerance  $h_{a,31}^{sh,1}$  of the system SH1 did not agree with the cross  
 447 accelerance  $h_{a,13}^{sh,3}$  of the system SH3. This is due to the change in location of the hammer  
 448 operator.



449 Fig. 21 Measured cross accelerances  $h_{a,13}^s$  and  $h_{a,31}^s$  of the empty bridge: (a) Magnitude; (b) Phase



450 Fig. 22 Measured cross accelerances  $h_{a,31}^{sh,1}$  and  $h_{a,13}^{sh,3}$ : (a) Magnitude; (b) Phase

#### 4.2.2. The elimination of the effect of the time delay of the measurement system

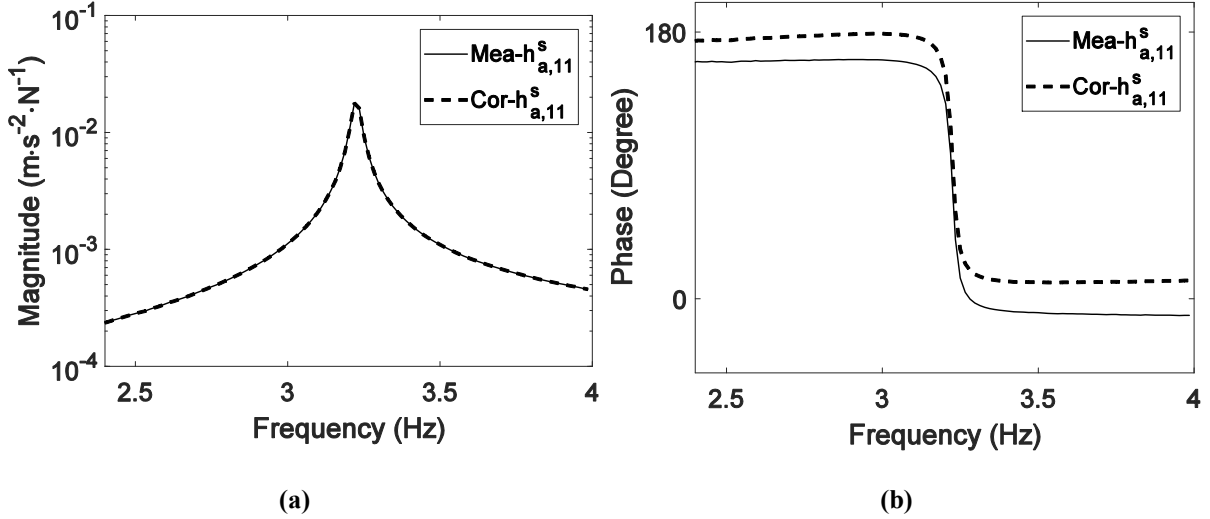
Fig. 21(b) and Fig. 22(b) show that there was a phase shift at low frequencies (below 8 Hz) in the measured accelerances of the empty bridge and the hammer operator-bridge systems, indicating a time delay in the acceleration measurement compared to the impulse force measurement. By contrast, there was no time delay observed in the accelerance measurement in the shaker testing presented in Section 4.1.1. It is noted that three QA750 accelerometers were used for the response measurement in both the impact hammer testing and the shaker testing. While a load cell (an integral piezoelectric force sensor of low impedance voltage mode type) at the tip of an hammer Dytran Model 5803A was used for impulse force measurement, a QA750 accelerometer was used in the shaker testing to measure the excitation force. The time delay in the low frequency range in measured accelerances from the impact hammer testing was mainly due to the difference between the time constant of the load cell for force measurement and that of the accelerometer for response measurement [36]. In the shaker testing, these two time constants are equal, and therefore they do not affect measured accelerances [36]. Appendix B demonstrates that this time delay affects the estimation of actual accelerances of the system under test but not eigenvalues. The effect of the time delay must be corrected for accurate subsystem identification since the proposed theory for the dynamic identification of the human body (i.e. Eq.(9)) and the empty structure (i.e. Eqs. (1) and (2)) requires the estimation of actual accelerances of the human-structure system.

Eq. (26) in Appendix B shows that measured accelerances should be multiplied by  $e^{\tau s}$ , where  $\tau$  (s) is the time delay of the measurement system. For the data acquisition system used in the impact hammer testing, an averaged time delay around the first mode may be approximately estimated as

$$\tau = \frac{\theta}{360f_1} \quad (17)$$

where  $\theta$  (degree) is the averaged delayed phase angle and  $f_1$  (Hz) is the natural frequency of the first mode. For example, the averaged delayed phase angle for the measured accelerance  $h_{a,11}^s$  of the empty bridge was 19 degrees. The natural frequency was estimated to be 3.22 Hz. The time delay was calculated as 0.0164 s using Eq. (17). The comparison of the measured accelerance  $h_{a,11}^s$  (thin solid line) and its phase corrected counterpart (thick dashed line) is displayed in Fig. 23. It can be seen that the phase has been corrected such that the phase angle

481 is almost 180 degrees before the phase drop at the fundamental frequency, while there are no  
 482 changes of the eigenvalues and magnitude of the FRF. In addition, it is reasonable to assume  
 483 that all the measured accelerances had the same time delay since the same measurement system  
 484 was used throughout the impact hammer testing.



485 **Fig. 23 Comparison of the measured acceleration  $h_{a,11}^s$  and its phase corrected counterpart: (a)**  
 486 **Magnitude; (b) Phase**

#### 487 4.2.3. The identification of the dynamics of the hammer operator and the empty bridge

488 After phase correction, the measured direct acceleration  $h_{a,11}^{sh,1}$  was curve fitted around the first  
 489 mode using the rational fraction polynomial method [35]. The estimated eigenvalues were  
 490  $\mu_{1,2}^{sh,1} = -0.1930 \pm 20.0834i \text{ s}^{-1}$  (the corresponding natural frequency and damping ratio were  
 491 3.20 Hz and 0.96%), and the corresponding analytical expression was

$$492 \quad h_{a,11}^{sh,1}(s) = \frac{a_0 s^2 + a_1 s + a_2}{b_0 s^2 + b_1 s + b_2} \quad (18)$$

493 where  $a_0 = 1.4493 \times 10^{-4}$ ,  $a_1 = -3.1393 \times 10^{-4} \text{ s}^{-1}$ ,  $a_2 = -0.0101 \text{ s}^{-2}$ ,  $b_0 = 1.1569$   
 494  $\text{N} \cdot \text{s}^2 \cdot \text{m}^{-1}$ ,  $b_1 = 0.4466 \text{ N} \cdot \text{s} \cdot \text{m}^{-1}$  and  $b_3 = 466.6605 \text{ N} \cdot \text{m}^{-1}$ .

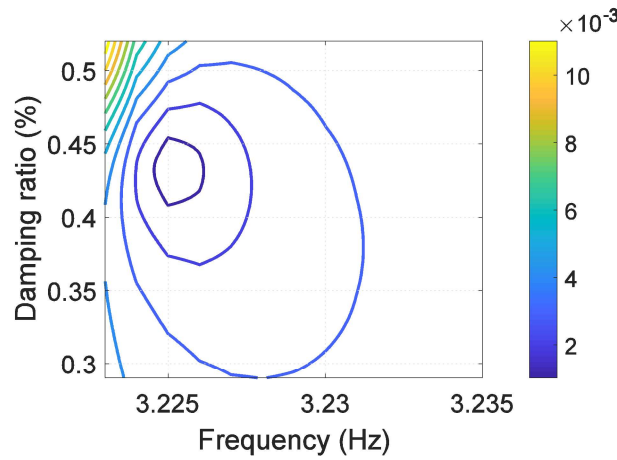
495 Similarly, the phase corrected  $h_{a,33}^{sh,3}$  was curved fitted and the eigenvalues were identified to be  
 496  $\mu_{1,2}^{sh,3} = -0.1030 \pm 20.2371i \text{ s}^{-1}$  (natural frequency and damping ratio were 3.22 Hz and  
 497 0.51%). Its analytical expression was

$$498 \quad h_{a,33}^{sh,3}(s) = \frac{a_0 s^2 + a_1 s + a_2}{b_0 s^2 + b_1 s + b_2} \quad (19)$$



499 Where  $a_0 = 2.9953 \times 10^{-5}$ ,  $a_1 = -1.1264 \times 10^{-4} \text{ s}^{-1}$ ,  $a_2 = -0.0581 \text{ s}^{-2}$ ,  $b_0 = 8.0321$   
 500  $\text{N}\cdot\text{s}^2\cdot\text{m}^{-1}$ ,  $b_1 = 1.6684 \text{ N}\cdot\text{s}\cdot\text{m}^{-1}$  and  $b_2 = 3289.7 \text{ N}\cdot\text{m}^{-1}$ .

501 With  $\mu_{1,2}^{sh,3}$  or the points around the minimum point shown in Fig. 24 as the initial guesses,  
 502  $\mu_{1,2}^s = -0.0868 \pm 20.2622i \text{ s}^{-1}$  were found to be the common zeros of  $\Delta h^{13}(s)$ ,  $\Delta h^{12}(s)$  and  
 503  $\Delta h^{23}(s)$ , which confirms that  $\mu_{1,2}^s$  were the eigenvalues of the empty bridge. The  
 504 corresponding natural frequency and damping ratio of the empty bridge were found to be 3.22  
 505 Hz and 0.43%, which agree with those identified from accelerances directly measured on the  
 506 empty bridge.



507

508 **Fig. 24 The magnitude of  $\Delta h^{13}(s)$  against frequency and damping ratio**

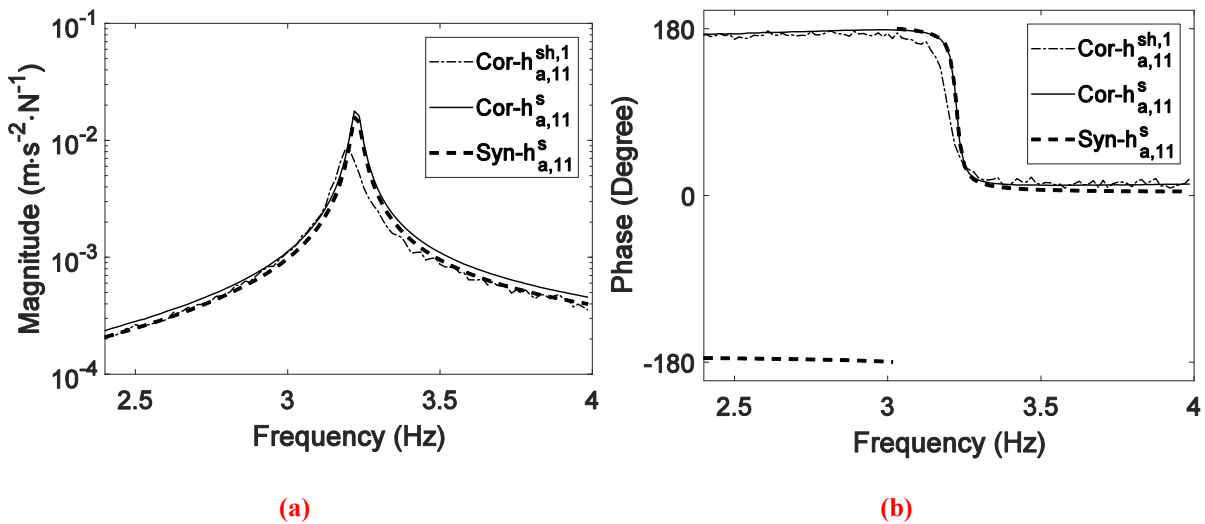
509 By using the eigenvalues  $\mu_{1,2}^s$ ,  $m_h = 62 + 5.5 = 67.5 \text{ kg}$ , Eq. (11) and Eq.(18), the human  
 510 body dynamics were identified as

$$511 \begin{bmatrix} c_h \\ k_h \end{bmatrix} = \begin{bmatrix} \mu_1^s & 1 \\ \mu_2^s & 1 \end{bmatrix}^{-1} \begin{bmatrix} \frac{(\mu_1^s)^2 m_h}{m_h h_{a,11}^{sh,1}(\mu_1^s) - 1} \\ \frac{(\mu_2^s)^2 m_h}{m_h h_{a,11}^{sh,1}(\mu_2^s) - 1} \end{bmatrix} = \begin{bmatrix} 8.86 \times 10^2 \text{ N} \cdot \text{s} \cdot \text{m}^{-1} \\ 3.71 \times 10^4 \text{ N} \cdot \text{m}^{-1} \end{bmatrix} \quad (20)$$

512 from which the natural frequency and damping ratio of the human occupant operating a  
 513 hammer in a crouching posture were calculated to be 3.73 Hz and 28%.

514 With the identified human body dynamics and the analytical expression of the phase corrected  
 515  $h_{a,11}^{sh,1}(s)$  given by Eq.(18), Eq. (1) gives the direct accelerance at TP1 of the empty structure.  
 516 Fig. 25 shows that the synthesised accelerance  $h_{a,11}^s(s)$  (thick dashed line) agrees reasonably

517 well with the measured counterpart of the empty bridge with phase corrected (thin solid line).  
 518 The comparison of the identified frequencies and damping ratios of the hammer operator-  
 519 bridge systems and the empty bridge indicates that the presence of the hammer operator causes  
 520 the decrease of the natural frequency of the empty bridge and the increase of the damping ratio.  
 521 This also explains the difference between the phase corrected accelerance of the hammer-  
 522 operator system (thin dash-dotted line) and that of the empty bridge shown in Fig. 25. Similarly,  
 523 other accelerances of the empty bridge can be synthesised by eliminating the effect of the  
 524 hammer operator.



525 **Fig. 25 Comparison of the synthesised accelerance of the empty bridge and the phase corrected**  
 526 **accelerances measured on the empty bridge and the human-bridge system: (a) Magnitude; (b) Phase**

## 527 5. Conclusions

528 A novel method for subsystem identification in a human-structure system has been proposed.  
 529 It enables the identification of the dynamic properties of the human body and the empty  
 530 structure from measured FRFs of the human-structure system. The proposed theory is verified  
 531 by a numerical example and two experimental case studies. The method is especially relevant  
 532 to the elimination of the effect of the hammer operator in manually operated impact hammer  
 533 testing on lightweight civil engineering structures. **In addition, the method can be generalised**  
 534 **to compensate for the effects of the shaker in shaker testing.** Furthermore, the time delay  
 535 between the force and response signals on the measured FRFs of the structure under test are  
 536 discussed, and appropriate strategies for their correction are proposed. **The proposed method,**  
 537 **which focuses on the presence of a single human occupant on lightweight low-frequency**  
 538 **structures (up to 8 Hz) in this paper, will be extended to the crowd-structure interaction in the**  
 539 **future work.**

540

541 **Appendix A: The elimination of the effect of shaker on measured FRFs of the empty**  
542 **structure**

543 The method for the elimination of the effect of a human occupant on the dynamic identification  
544 of the empty structure presented in the paper [18] can be extended to the elimination of the  
545 effect of shaker on measured FRFs. Under the assumption that a shaker is a mass block of the  
546 total mass  $m_e$ , the resultant formulas are the same as those used for the elimination of  
547 transducer mass loading effects in some studies [37, 38]. Hence, the derivation of the formulas  
548 is not presented here, instead they are shown in the final form.

549 Namely, the direct receptance at the  $p$ -th DOF ( $p \leq n$ ) of the empty structure  $h_{pp}^s(s)$  and that  
550 of the structure with the shaker at the  $p$ -th DOF  $h_{pp}^{se,p}(s)$  are related by

551 
$$h_{pp}^s(s) = \frac{h_{pp}^{se,p}(s)}{1 - m_e s^2 h_{pp}^{se,p}(s)} \quad (21)$$

552 Similarly, the cross receptance between the  $q$ -th DOF ( $p \leq n$ ) and the  $p$ -th DOF of the empty  
553 structure  $h_{qp}^s(s)$  and that of the structure with the shaker at the  $p$ -th DOF  $h_{qp}^{se,p}(s)$  are related  
554 by

555 
$$h_{qp}^s(s) = \frac{h_{qp}^{se,p}(s)}{1 - m_e s^2 h_{qp}^{se,p}(s)} \quad (22)$$

556 **Appendix B: The effect of the time delay of the measurement system on measured FRFs**

557 The equation of forced vibration of a linear structure having  $n$  DOFs may be written in the  
558 Laplace domain as

559 
$$\mathbf{x}_s(s) = \mathbf{H}_s(s) \mathbf{f}_s(s) \quad (23)$$

560 where  $\mathbf{H}_s(s)$  is the receptance matrix,  $s$  is the Laplace variable, whilst  $\mathbf{x}_s(s)$  and  $\mathbf{f}_s(s)$  are the  
561 Laplace transforms of displacement and force vectors.

562 In the modal testing of the above system, if the measurement system is an ideal system but  
563 there is a time delay,  $\tau$ , between the response and force signal measurement, then the  
564 measurement system FRF can be expressed as  $e^{-\tau s}$ . The equation of forced vibration of the  
565 structure combined with the measurement system then becomes

$$566 \quad \tilde{\mathbf{x}}_s(s) = \mathbf{H}_s(s)e^{-\tau s} \mathbf{f}_s(s) \quad (24)$$

567 where  $\tilde{\mathbf{x}}_s(s)$  is the Laplace transform of the measured output of the structure combined with  
568 the measurement system.

569 The measured receptance then becomes

$$570 \quad \tilde{\mathbf{H}}_s(s) = \frac{\tilde{\mathbf{x}}_s(s)}{\mathbf{f}_s(s)} = \mathbf{H}_s(s)e^{-\tau s} \quad (25)$$

571 which shows that the actual receptance of the structure may be obtained by correcting the  
572 measured receptance by

$$573 \quad \mathbf{H}_s(s) = \tilde{\mathbf{H}}_s(s)e^{\tau s} \quad (26)$$

#### 574 ACKNOWLEDGMENT

575 This research was supported by the UK Engineering and Physical Sciences Research Council  
576 [grant number EP/M021505/1: Characterising dynamic performance of fibre reinforced  
577 polymer structures for resilience and sustainability].

#### 578 DATA AVAILABILITY

579 Electronic format of the data collected in this research can be downloaded freely from the  
580 University of Warwick webpages <http://wrap.warwick.ac.uk/108822>.

581

#### 582 References

583

- 584 [1] B.R. Ellis, T. Ji, Human-structure interaction in vertical vibrations, Proceedings of the  
585 Institution of Civil Engineers - Structures and Buildings, 122 (1997) 1-9.
- 586 [2] R. Sachse, A. Pavic, P. Reynolds, Parametric study of modal properties of damped two-  
587 degree-of-freedom crowd-structure dynamic systems, Journal of Sound and Vibration, 274  
588 (2004) 461-480.
- 589 [3] J.M.W. Brownjohn, Energy dissipation from vibrating floor slabs due to human-structure  
590 interaction, Shock and Vibration, 8 (2001).
- 591 [4] S. Živanović, I. Diaz, A. Pavić, Influence of walking and standing crowds on structural  
592 dynamic properties, in: Proceeding of Conference & Exposition on Structural Dynamics  
593 (IMAC XXVII), 2009.
- 594 [5] J. Sim, Human-structure interaction in cantilever grandstands, PhD Thesis, The University  
595 of Oxford 2006.
- 596 [6] R. Sachse, A. Pavic, P. Reynolds, Human-structure dynamic interaction in civil engineering  
597 dynamics: A literature review, Shock and Vibration Digest, 35 (2003) 3-18.
- 598 [7] S. Živanović, A. Pavic, P. Reynolds, Vibration serviceability of footbridges under human-  
599 induced excitation: a literature review, Journal of Sound and Vibration, 279 (2005) 1-74.
- 600 [8] S. Živanović, G. Feltrin, J.T. Mottram, J.M.W. Brownjohn, Vibration performance of  
601 bridges made of fibre reinforced polymer, in: F.N. Catbas (Ed.) Dynamics of Civil Structures,  
602 Volume 4: Proceedings of the 32nd IMAC, A Conference and Exposition on Structural  
603 Dynamics, 2014, Springer International Publishing, Cham, 2014, pp. 155-162.
- 604 [9] E. Shahabpoor, A. Pavic, V. Racic, Interaction between walking humans and structures in  
605 vertical direction: a literature review, Shock and Vibration, 2016 (2016) 22.
- 606 [10] R.O. Foschi, G.A. Neumann, F. Yao, B. Folz, Floor vibration due to occupants and  
607 reliability-based design guidelines, Canadian Journal of Civil Engineering, 22 (1995) 471-479.
- 608 [11] Y. Matsumoto, M.J. Griffin, Dynamic response of the standing human body exposed to  
609 vertical vibration: Influence of posture and vibration magnitude, Journal of Sound and  
610 Vibration, 212 (1998) 85-107.
- 611 [12] L. Wei, M.J. Griffin, Mathematical models for the apparent mass of the seated human  
612 body exposed to vertical vibration, Journal of Sound and Vibration, 212 (1998) 855-874.
- 613 [13] X. Zheng, J.M.W. Brownjohn, Modeling and simulation of human-floor system under  
614 vertical vibration, in: L.P. Davis (Ed.) Proc. SPIE 4327, Smart Structures and Materials 2001:  
615 Smart Structures and Integrated Systems, Newport Beach, CA, USA, 2001, pp. 513-520.
- 616 [14] R. Sachse, The influences of human occupants on the dynamic properties of slender  
617 structures, PhD Thesis, University of Sheffield, 2003.
- 618 [15] K. Van Nimmen, K. Maes, S. Zivanovic, G. Lombaert, G. De Roeck, P. Van den Broeck,  
619 Identification and modelling of vertical human-structure interaction, in: J. Caicedo, S. Pakzad  
620 (Eds.) Dynamics of Civil Structures, Volume 2: Proceedings of the 33rd IMAC, A Conference  
621 and Exposition on Structural Dynamics, 2015, Springer International Publishing, Cham, 2015,  
622 pp. 319-330.
- 623 [16] E. Shahabpoor, A. Pavic, V. Racic, Identification of mass-spring-damper model of  
624 walking humans, Structures, 5 (2016) 233-246.
- 625 [17] E. Shahabpoor, A. Pavic, V. Racic, Identification of walking human model using agent-  
626 based modelling, Mechanical Systems and Signal Processing, 103 (2018) 352-367.

- 627 [18] X. Wei, S. Živanović, Frequency response function-based explicit framework for dynamic  
628 identification in human-structure systems, *Journal of Sound and Vibration*, 422 (2018) 453-  
629 470.
- 630 [19] J. Sim, A. Blakeborough, M. Williams, Modelling effects of passive crowds on grandstand  
631 vibration, *Proceedings of the Institution of Civil Engineers - Structures and Buildings*, 159  
632 (2006) 261-272.
- 633 [20] C.A. Jones, P. Reynolds, A. Pavic, Vibration serviceability of stadia structures subjected  
634 to dynamic crowd loads: A literature review, *Journal of Sound and Vibration*, 330 (2011) 1531-  
635 1566.
- 636 [21] C.C. Caprani, E. Ahmadi, Formulation of human–structure interaction system models for  
637 vertical vibration, *Journal of Sound and Vibration*, 377 (2016) 346-367.
- 638 [22] J.W. Qin, S.S. Law, Q.S. Yang, N. Yang, Finite element analysis of pedestrian-bridge  
639 dynamic interaction, *Journal of Applied Mechanics*, 81 (2013) 041001-041001-041015.
- 640 [23] A. Pavic, R. Pimentel, P. Waldron, Instrumented sledge hammer impact excitation:  
641 worked examples, in: *Proceedings-Spie the International Society for Optical Engineering*,  
642 Spie The International Society for Optica, 1998, pp. 929-935.
- 643 [24] D. Tirelli, Modal analysis of small & medium structures by fast impact hammer testing  
644 method, in, 2011.
- 645 [25] S. Živanović, X. Wei, J. Russell, J.T. Mottram, Vibration performance of two FRP  
646 footbridge structures in the United Kingdom, in: *Footbridge 2017*, Berlin, Germany, 2017.
- 647 [26] M.G.R. Toward, M.J. Griffin, Apparent mass of the human body in the vertical direction:  
648 Inter-subject variability, *Journal of Sound and Vibration*, 330 (2011) 827-841.
- 649 [27] Y. Matsumoto, M.J. Griffin, Mathematical models for the apparent masses of standing  
650 subjects exposed to vertical whole-body vibration, *Journal of Sound and Vibration*, 260 (2003)  
651 431-451.
- 652 [28] IStructE/DTLR/DCMS, Dynamic performance requirements for permanent grandstands  
653 subject to crowd action, recommendations for management, design and assessment, The  
654 Institution of Structural Engineers (IStructE), London, 2008.
- 655 [29] A. Pavic, P. Reynolds, Experimental verification of novel 3DOF model for grandstand  
656 crowdstructure dynamic interaction, in: *26th international modal analysis conference: IMAC-*  
657 *XXVI*, Orlando, Florida, 2008.
- 658 [30] C.A. Jones, A. Pavic, P. Reynolds, R.E. Harrison, Verification of equivalent mass–spring–  
659 damper models for crowd–structure vibration response prediction, *Canadian Journal of Civil*  
660 *Engineering*, 38 (2011) 1122-1135.
- 661 [31] K.A. Salyards, N.C. Noss, Experimental evaluation of the influence of human-structure  
662 interaction for vibration serviceability, *Journal of Performance of Constructed Facilities*, 28  
663 (2014) 458-465.
- 664 [32] T. Coleman, Y. Li, An interior trust region approach for nonlinear minimization subject  
665 to bounds, *SIAM Journal on Optimization*, 6 (1996) 418-445.
- 666 [33] ISO, ISO 5982:1981 Vibration and shock -- Mechanical driving point impedance of the  
667 human body, International Organisation for Standardisation (ISO), Geneva, Switzerland, 1981.
- 668 [34] Z. Friedman, J.B. Kosmatka, An improved two-node Timoshenko beam finite element,  
669 *Computers & Structures*, 47 (1993) 473-481.

- 670 [35] M.H. Richardson, D.L. Formenti, Parameter estimation from frequency response  
671 measurements using rational fraction polynomials, in: the 1st International Modal Analysis  
672 Conference, Orlando, FL, 1982.
- 673 [36] K.G. McConnell, P.S. Varoto, *Vibration testing: theory and practice*, Wiley, New Jersey,  
674 2008.
- 675 [37] J.M.M. Silva, N.M.M. Maia, A.M.R. Ribeiro, Cancellation of mass-loading effects of  
676 transducers and evaluation of unmeasured frequency response functions, *Journal of Sound and*  
677 *Vibration*, 236 (2000) 761-779.
- 678 [38] O. Cakar, K.Y. Sanliturk, Elimination of transducer mass loading effects from frequency  
679 response functions, *Mechanical Systems and Signal Processing*, 19 (2005) 87-104.

680